Analytica Chimica Acta 1127 (2020) 122–130

Contents lists available at ScienceDirect

Analytica Chimica Acta

journal homepage: www.elsevier.com/locate/aca

Ultrasensitive microfluidic electrochemical immunosensor based on electrodeposited nanoporous gold for SOX-2 determination

Matías Regiart [a], Alba Marina Gimenez [b], Alexandre T. Lopes [c], Marcelo N.P. Carreño [c], Mauro Bertotti [a, *]

[a] Department of Fundamental Chemistry, Institute of Chemistry, University of São Paulo, Av. Prof. Lineu Prestes 748, 05508-000, São Paulo, SP, Brazil
[b] Department of Clinical and Toxicological Analyses, School of Pharmaceutical Sciences, University of São Paulo, 05508-000, São Paulo, SP, Brazil
[c] Department of Electronic Systems Engineering, Polytechnic School, University of São Paulo, 05508-010, São Paulo, SP, Brazil

HIGHLIGHTS

- An ultrasensitive and portable microfluidic electrochemical immunosensor for SOX-2 cancer biomarker detection was developed.
- Selectivity and sensitivity were improved by a physical-chemical channel treatment in order to obtain a hydrophilicity functional platform.
- The gold electrode was modified by using a dynamic hydrogen bubble template method, resulting in a gold nanoporous electrode.
- SOX-2 present in the sample was detected by a type sandwich immunoassay.

GRAPHICAL ABSTRACT

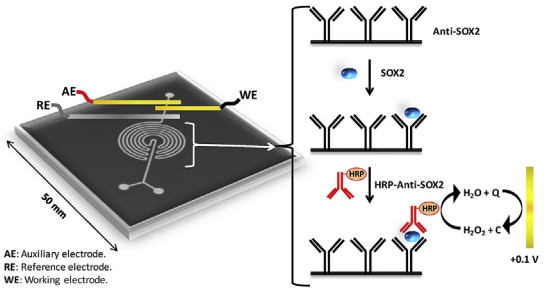

ARTICLE INFO

Article history:
Received 28 May 2020
Received in revised form
10 June 2020
Accepted 15 June 2020
Available online 8 July 2020

Keywords:
Microfluidic
Electrochemical
Immunosensor
SOX-2
Gold nanoporous

ABSTRACT

An ultrasensitive and portable microfluidic electrochemical immunosensor for SOX-2 cancer biomarker determination was developed. The selectivity and sensitivity of the sensor were improved by modifying the microfluidic channel. This was accomplished through a physical-chemical treatment to produce a hydrophilic surface, with an increased surface to volume/ratio, where the anti-SOX-2 antibodies can be covalently immobilized. A sputtered gold electrode was used as detector and its surface was activated by using a dynamic hydrogen bubble template method. As a result, a gold nanoporous structure (NPAu) with outstanding properties, like high specific surface area, large pore volume, uniform nanostructure, good conductivity, and excellent electrochemical activity was obtained.

SOX-2 present in the sample was bound to the anti-SOX-2 immobilized in the microfluidic channel, and then was labeled with a second antibody marked with horseradish peroxidase (HRP-anti-SOX-2) like a sandwich immunoassay. Finally, an H_2O_2 + catechol solution was added, and the enzymatic product (quinone) was reduced on the NPAu electrode at +0.1 V (vs. Ag). The current obtained was directly proportional to the SOX-2 concentration in the sample. The detection limit achieved was 30 pg mL^{-1}, and the coefficient of variation was less than 4.75%. Therefore, the microfluidic electrochemical immunosensor is a suitable clinical device for *in situ* SOX-2 determination in real samples.

* Corresponding author.
E-mail address: mbertott@iq.usp.br (M. Bertotti).

https://doi.org/10.1016/j.aca.2020.06.037
0003-2670/

1. Introduction

In recent years, the study of tumor biomarkers has become essential to detect and control different kinds of cancer [1]. Biomarkers are molecules found in various fluids, such as saliva, serum, tissues, among others, and they allow to control if the biological conditions of the patient are normal or abnormal. In this way, the monitoring of the biomarkers concentration can serve as a powerful tool for rapid detection of a disease, as well as helps to control the evolution of the patient's condition during the treatment, thus improving the chances of recovery [2].

SOX-2 is a protein also known as SRY-box 2 (Sex determining Region Y-box 2) and is a transcription factor whose function is essential to maintain the self-renewal of undifferentiated embryonic stem cells. The SOX-2 protein is encoded by a gene that has no introns and belongs to the family of SOX HMG-box transcription factors related to SRY, which are involved in the regulation of embryonic development, in the cell differentiation, and in the induction of stem cells pluripotentiality [3,4]. Several mutations in this gene have been associated with a severe malformation in the eye structure called anophthalmia. It has also been determined that ectopic expression of SOX-2 could be related to abnormal differentiation of colorectal cancer cells [5], as well as to overexpression in breast [6], ovarian [7], lung [8], esophageal [9], prostate [10], pancreatic [11], testicular [12], and skin/neck/head squamous cell carcinoma, among others [13,14].

Taking into account the issues mentioned above, the development of a sensitive, selective, fast, and portable device to detect SOX-2 in human serum samples is imperative. SOX-2 determination can be accomplished by commercial enzyme immunoassays (ELISA), but they have disadvantages such as long analysis time, require specialized labor, are expensive, and do not have adequate sensitivity for SOX-2 determination in real samples [15].

Electrochemical immunosensors can be classified as non-labeled (or label-free) and labeled (or sandwich-type) immunosensors [16]. So far, two label-free electrochemical immunosensors have been reported for the SOX-2 biomarker determination. Aydin and Sezgintürk developed a disposable immunosensor for SOX-2 detection based on an indium tin oxide (ITO) electrode modified with carboxyethylsilanetriol (CTES) for the anti-SOX-2 antibody immobilization. An insulating layer was formed owing to the antigen-antibody interaction, and such layer prevents the interfacial electron transfer kinetics between a redox probe and the electrode, producing an increase in the electron-transfer resistance which is proportional to the target analyte concentration [17]. Also, Özcan and Sezgintürk developed an immunosensor using an indium tin oxide-polyethylene terephthalate (ITO-PET) working electrode, which was subsequently modified with 11-cyanoundecyltrimethoxysilane (11-CUTMS). Then, the anti-SOX-2 was immobilized, and the SOX-2 was indirectly detected by EIS using $K_3[Fe(CN)_6]/K_4[Fe(CN)_6]$ as a probe [18].

In general, label-free immunosensors have lower sensitivity and selectivity compared to sandwich-type immunosensors. Besides, the analytical performance of the sandwich-type immunosensors could be improved [16]. In this way, microfluidic devices with electrochemical detection are an exciting approach due to their benefits, such as robustness, low samples, and reagents consumption, short analysis time, simplicity, portability, and low detection limit [19]. Furthermore, the microfluidic channel surface can be modified in order to improve the selectivity and sensitivity of the determinations, and this can be accomplished by a physical-chemical treatment to generate functional groups that can serve as a functional platform for the biomolecules immobilization [20,21].

In the present work, we have developed the first microfluidic electrochemical immunosensor for SOX-2 cancer biomarker determination in real samples. The gold electrode surface was modified with a gold nanoporous (NPAu) layer by using a dynamic hydrogen bubble template (DHBT) method based on the production of hydrogen bubbles simultaneously with the metal ions reduction/deposition [22]. The hydrogen bubbles evolution provides a dynamic template for the metal electrodeposition, creating three-dimensional nanoarchitecture porous materials. The electrodeposition parameters such as time and potential strongly influence the pore size and film density [23]. Hence, detection platforms with outstanding properties, including high specific surface area, large pore volume, uniform nanostructure, unique biocompatibility, good conductivity, and excellent electrochemical activity, can be fabricated by fine control of the experimental conditions [24]. The physical-chemical modification performed in the microfluidic channel was studied by Infrared spectroscopy (IR), and the NPAu film was further characterized by Scanning electron microscopy (SEM), Energy dispersive spectrometry (EDS), Cyclic voltammetry (CV), and X-ray diffraction (XRD).

2. Experimental

2.1. Materials and reagents

All reagents used were of analytical reagent grade. $HAuCl_4$, bovine serum albumin (BSA), 3-aminopropyl-triethoxysilane (APTES), glutaraldehyde (GLU), and catechol were acquired from Sigma-Aldrich, St. Louis, USA. Phosphate buffer saline (PBS pH 7.00), H_2O_2, acetic acid, and H_2SO_4 were purchased from Merck (Darmstadt, Germany). SU-8 (3025 series) photo resin and Sylgard 184 Poly(dimethylsiloxane) (PDMS prepolymer + curing agent) were obtained from Clariant Corporation (Sommerville, USA) and Dow Corning (Midland, USA), respectively. The enzyme immunoassay for the quantitative determination of SOX-2 was purchased from Abcam (USA) and used according to the manufacturer's instructions. All the other reagents employed were of analytical grade and were used without further purification. Aqueous solutions were prepared by using purified water from a Milli-Q system.

2.2. Apparatus

Amperometric and voltammetric measurements were performed using a PGSTAT128 N potentiostat from Methrohm Autolab (Metrohm, Netherlands), with a NOVA 1.11 electrochemical analysis software. Electrochemical measurements were carried out using an electrochemical cell obtained by sputtering, as it can be seen in section "2.3. Microfluidic device fabrication", with a three-electrodes system (gold auxiliary and working (GE) electrodes, and a silver reference electrode), at room temperature. All the potentials were referred to Ag. Sputtering metal deposition was carried out in an SPI-Module Sputter Coater (Structure Probe Inc, West Chester, PA). The electrode thickness was controlled with a Quartz Crystal Thickness Monitor model 12,161 equipment (SPI-Module, Structure Probe Inc, West Chester, PA).

The NPAu surface morphology was investigated by scanning electron microscope images using a Jeol-JSM 7401F (FEG) (Jeol, Japan) instrument equipped with an Energy Dispersive Spectroscopy analysis FEI Helios Nanolab 660 module. The NPAu crystallographic orientation was studied by X-ray diffraction in a BrukerD2 Phaser X-ray diffractometer, equipped with a Cu Kα source ($\lambda = 1.5418$ Å) (Bruker, UK). PDMS functionalization was studied by

Infrared spectroscopy using a Bruker alpha ECO-ATR equipment (Bruker, UK).

A syringe pump was used to introduce the solutions in the microfluidic device (Pump System Inc., USA). Absorbance was measured with a Datamed Multiskan FC Thermo Scientific UV/VIS spectrophotometer (Datamed Brasil, São Paulo). All pH measurements were made with a Metrohm 827 pH lab (Metrohm Brasil, São Paulo).

2.3. Microfluidic device fabrication

The microfluidic device development involves three steps: i) The fabrication of microfluidic PDMS channels itself, ii) The deposition of metal electrodes on a glass plate, and iii) The sealing process between the PDMS device and the glass plate with the sputtered electrodes (Scheme 1). The microfluidic channel was fabricated by micro molding of liquid PDMS (Sylgard 184) on a 50 μm thick SU-8 mold (master) predefined on a silicon wafer (Scheme 1, A and B). The microfluidic channel geometry was designed in a CAD software and transferred to the SU-8 (3025 series) by conventional photolithography. The PDMS was prepared with elastomer and cure agent in a 10:1 ratio. After that, it was poured on the SU-8 mold. The material was then subjected to a vacuum degassing treatment to remove bubbles, followed by a curing step (at 80 °C for 30 min). After that, the cured PDMS was demolded from the SU-8 master and, after opening the outlet holes, it was ready to be attached to the glass plate with the electrodes. This was done by introducing the PDMS piece and the glass plate to a plasma treatment under N_2O atmosphere for 1 min, followed by the surfaces contact (Scheme 1, C). This leads to a secure, leak-free seal. The final step was a tube connection for the external fluid access (Scheme 1, D). The final device size was 5×5 cm^2 (Scheme 1, E).

Note that the microfluidic electrochemical immunosensor was

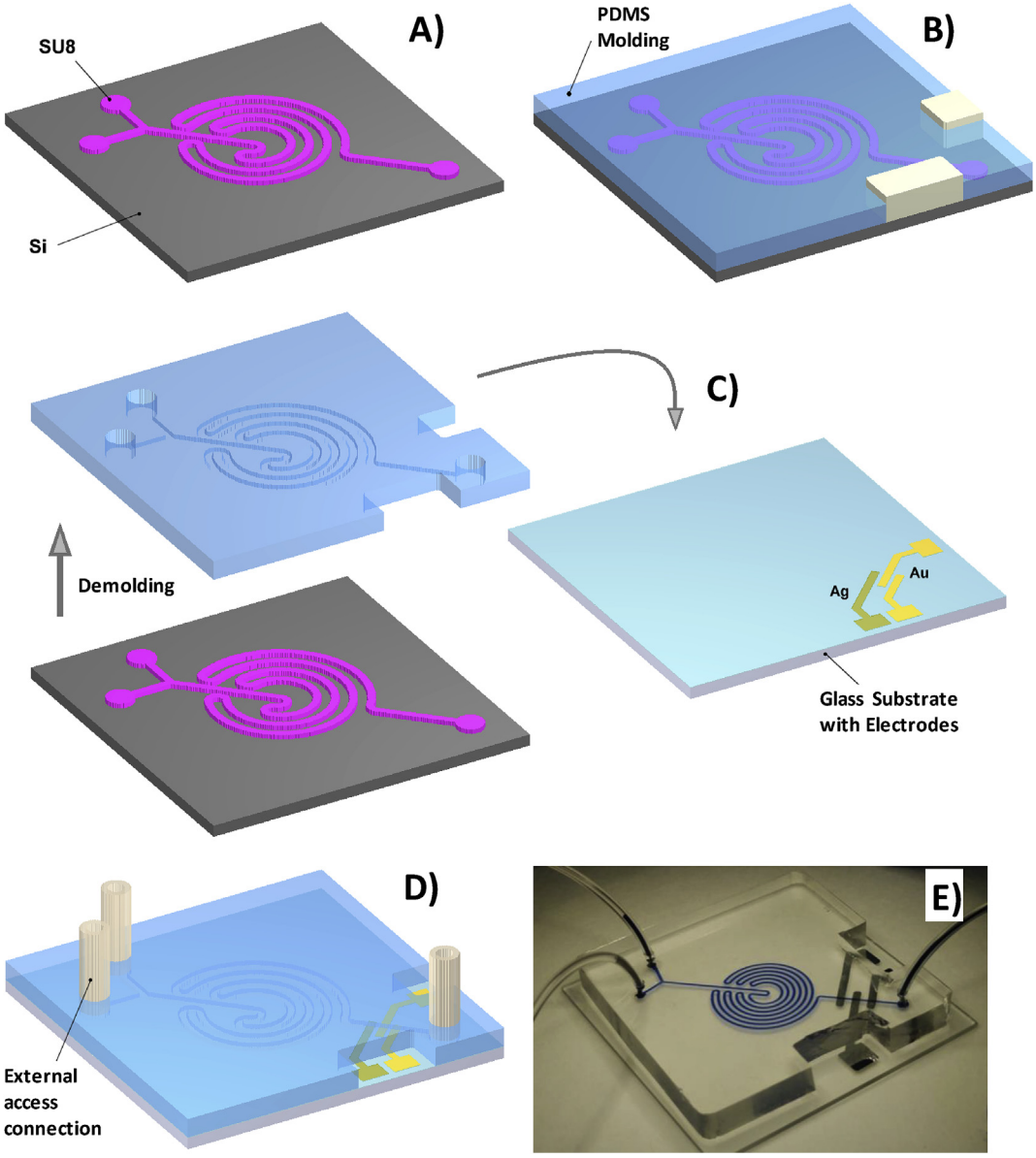

Scheme 1. Fabrication step sequence of the microfluidic immunosensor: A) SU-8 master with a thickness of 50 μm and the micro channels geometry, B) PDMS molding, C) Demolding and sealing on a glass plate containing Au and Ag electrodes, D) Tube connection for fluid input and output, and E) Final fabricated immunosensor.

manufactured according to a procedure previously reported [25] with some modifications (see Scheme 2). For the electrodes fabrication, a metal sheet patterned mask was employed. Firstly, the mask was positioned near to the output, followed by 20 nm titanium sputtering deposition in order to improve the metal adhesion to the glass. Then, layers of silver (100 nm) and gold (100 nm) were sputtered over the glass plate for the reference and working/auxiliary electrodes, respectively. Finally, the metal mask was removed, leaving the gold and silver electrodes on the glass. The electrode geometric area was 0.011 cm^2.

2.4. NPAu/GE preparation

Immediately after the microfluidic device sealing, the NPAu electrodeposition was carried out through a potentiostatic DHBT method by applying a fixed − 4 V potential for 150 s in a 1 mmol L^{-1} $HAuCl_4$ + 0.5 mol L^{-1} H_2SO_4 solution through hydrodynamic conditions (50 μL min^{-1} flow rate). The electrodeposition parameters (potential and time) were optimized according to a procedure previously reported [26], as it can be seen in the section "3.3. Optimization of experimental parameters". Later, the electrodeposited NPAu films were washed several times with water until pH: 7. The NPAu film was characterized by SEM, EDS, CV and XRD.

2.5. SOX-2 antibody immobilization in microfluidic channels surface

After the gold electrode modification, the PDMS was treated in order to modify the microfluidic channel with the SOX-2 antibody. The functionalization process was performed according to a previously reported procedure with some modifications [27]. An APTES solution (10% APTES:10% H_2O:80% Ethanol) was pumped into the microfluidic channel at 50 μL min^{-1} flow rate for 12 h, followed by several washing steps with water and ethanol. In this step, the APTES binds to the channel surface modified with hydroxylic groups, in a silanization process. Then, the channel was dried with argon gas.

After that, a 5% GLU solution in PBS pH 8.00 was pumped into the channel for 2 h, followed by a washing step with PBS pH 7.00. GLU acts as a crosslinker and binds the aldehyde group with the amine group of the APTES, leaving free an aldehyde group to react with the amine groups of the antibodies. Then, the channel was put in contact with the SOX-2 antibody (dilution 1:200 in 0.1 mol L^{-1} PBS pH 7.00) for 12 h at 4 °C. Finally, the channel was rinsed with 0.1 mol L^{-1} PBS pH 7.00 and stored at 4 °C. The immobilized antibody was stable for at least 1 month. The modification channel step was followed by IR. As it can be seen in Fig. 1 A), the PDMS IR showed the typical peaks at 797 cm^{-1} (−CH_3 rocking and Si−C stretching in Si−CH_3), 1018−1072 cm^{-1} (Si−O−Si stretching), 1256 cm^{-1} (CH_3 deformation in Si−CH_3), and 2965 cm^{-1} (asymmetric CH_3 stretching in Si−CH_3), in agreement with the literature [28,29]. The oxygen plasma generates a significant number of hydroxyl groups in the PDMS surface, as it can be observed by the broad band corresponding to the O−H stretching at 3382 cm^{-1} in the IR spectrum (Fig. 1 B). The typical amine group peaks at 690, 1321−1381, 1483, 1560, and 3200 cm^{-1} (N−H, N−O) were noticed in the IR spectrum after the APTES/PDMS modification. Moreover, after the GLU modification step, the typical carboxylic (C−O, O−H) and carbonyl (C═O) peaks were noted at 952, 1112, 1719, 2937 cm^{-1}.

2.6. Analytical procedure for SOX-2 determination

The microfluidic electrochemical immunosensor was applied to SOX-2 determination in five spiked samples. All solutions were injected at 5 μL min^{-1} flow rate. The procedure involved the following steps (Scheme 2).

Firstly, and in order to avoid unspecific bindings, a blocking treatment was performed using 1% BSA in 0.1 mol L^{-1} PBS pH 7.00 for 2 min, followed by a washing step with 0.1 mol L^{-1} PBS pH 7.00 for 2 min. Then, the sample (previously diluted 100-fold with 0.1 mol L^{-1} PBS pH 7.00) was pumped for 5 min, followed by a washing step to remove the non-binding material. In this step, the SOX-2 protein present in the sample binds to the anti-SOX-2 antibody immobilized in the PDMS surface. Later, the SOX-2 protein binds to a second antibody labeled with horseradish peroxidase (HRP-anti-SOX-2), which was pumped for 5 min. Finally, the substrate solution (1 mmol L^{-1} H_2O_2 + 1 mmol L^{-1} catechol in 0.1 mol L^{-1} acetic/acetate buffer pH 4.50) was pumped, and the enzymatic product (quinone) was detected in the NPAu/GE at + 0.1 V by amperometry. For instance, Fig. S1 shows a typical response of the NPAu/GE sensor coupled to the microfluidic

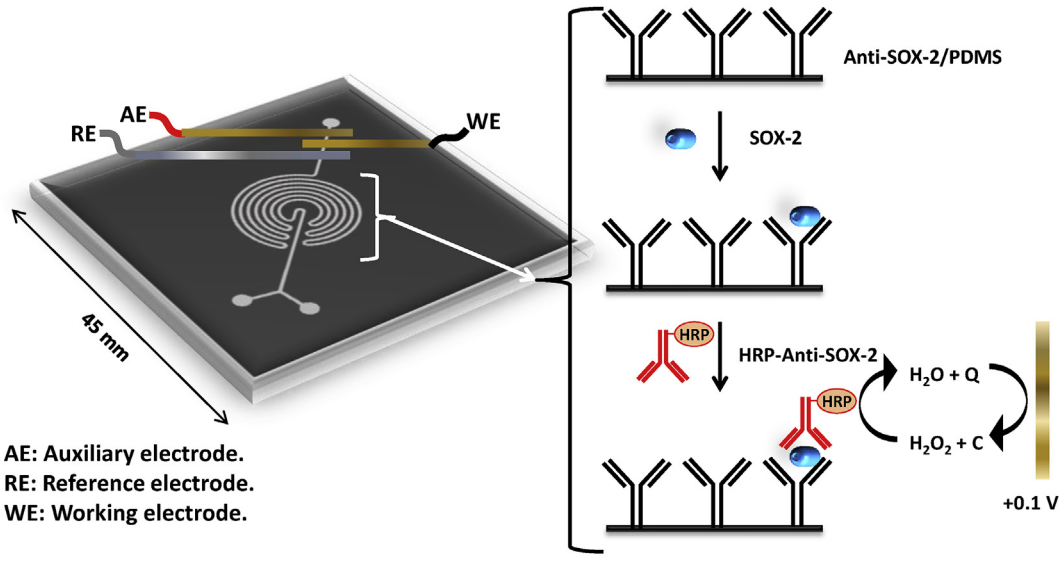

Scheme 2. Microfluidic electrochemical immunosensor for SOX-2 determination in real samples.

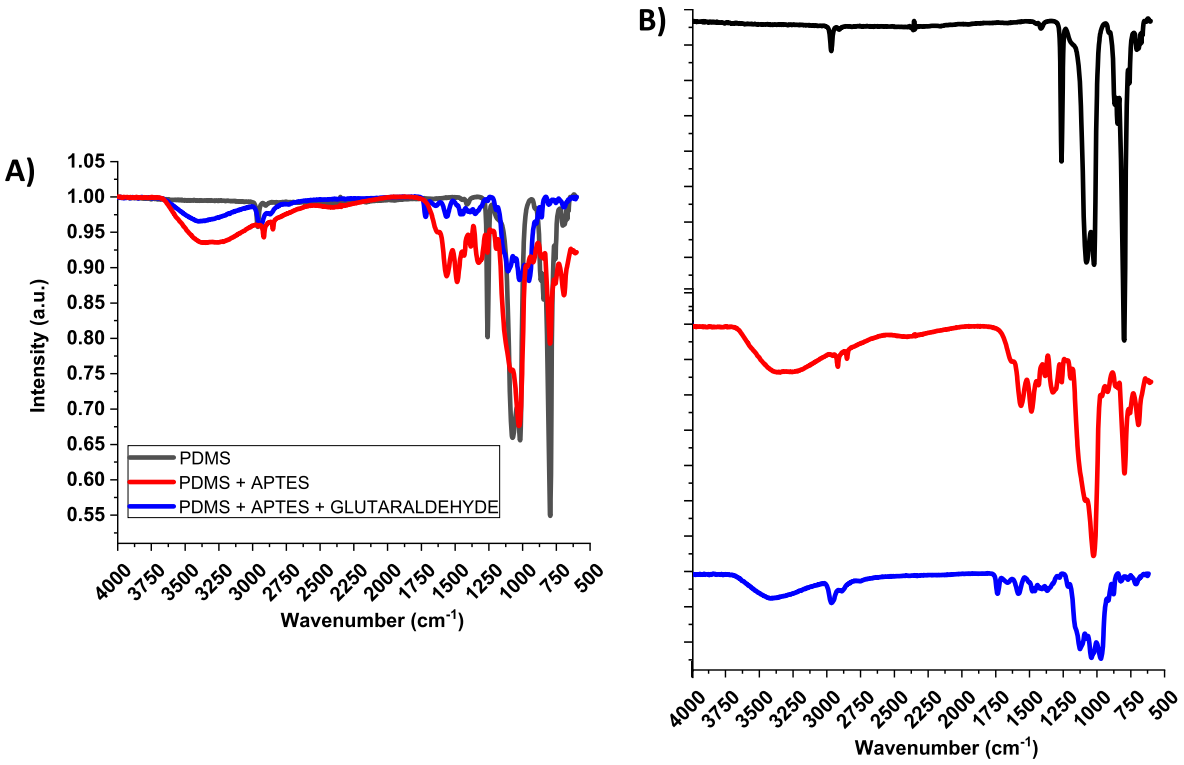

Fig. 1. A) Infrared spectroscopy study of the PDMS functionalized with 3-aminopropyl-triethoxysilane (APTES), and Glutaraldehyde (GLU), and B) Same spectra, but separated to allow better evaluation.

electrochemical immunosensor. The potential was selected according to the voltammograms recorded in a catechol solution, where the anodic oxidation of catechol to quinone ($E_{pa} = +0.40$ V) and the subsequent reduction process ($E_{pc} = +0.33$ V) can be observed in such reversible electrochemical process (Fig. 4 B). Hence, + 0.10 V is a suitable potential to detect quinone, the enzymatic product of the catechol oxidation.

Before each analysis, the immunosensor was put in contact with a 0.1 mol L^{-1} glycine pH 2.00 desorption buffer for 5 min, followed by a washing step with a 0.1 mol L^{-1} PBS pH 7.00 solution. This procedure unbinds the SOX-2 protein bound to the anti-SOX-2 antibodies, allowing to perform a new determination. The device can be used without significant loss of sensitivity for 1 month. The microfluidic immunosensor was stored in 0.1 mol L^{-1} PBS pH 7.00 at 4 °C when not in use.

3. Results and discussion

3.1. NPAu/GE morphology and composition characterization

The NPAu/GE morphology was characterized by SEM at several magnifications. Fig. 2 A) shows the bare gold electrode surface image, and a uniform gold nanoporous structure (honeycomb-like dendritic, HCLD) can be noticed in Fig. 2B) and C). The μm-size porous were produced by the electrogenerated H_2 bubbles during the gold electrodeposition, and they act as a dynamic template in the DBHT method. The HCLD film has an enhanced surface area, a large quantity of active sites, and a rough surface. Such surface imperfections/edges increase the electron transfer rate, enhancing the electrocatalytic activity, and playing an outstanding role in electrochemistry [26]. Fig. 2 D) shows films with highly-*branched and well-dispersed dendrite* structures.

Regarding the NPAu/GE elemental composition and in order to evaluate the chemical purity, an EDS spectrum was recorded and the Au typical peaks can be clearly observed in Fig. S2 A). A strong band characteristic of gold nanocrystals optical absorption involving the X-rays at 2.13 keV, and a low-intensity band corresponding to gold outer shells at 9.72 keV were noticed. Therefore, the electrodeposition process produces a high purity NPAu film.

The NPAu crystallographic orientation was characterized by XRD measurements. The XRD in Fig. S2 B) shows sharps diffraction peaks at 2θ (42.4, 50.2, and 68.8°) corresponding to the (111), (200), and (220) crystallographic planes. That is a clear evidence of the nanoporous gold structure formation.

3.2. NPAu/GE electrochemical characterization

In order to analyze the nanoporous gold electrochemical behavior, CVs of the GE and NPAu/GE were recorded in 0.5 mol L^{-1} H_2SO_4 from 0 to +1.7 V at 75 mV s^{-1} scan rate (Fig. 3 A). An increase in the gold oxidation current and the appearance of anodic peaks at + 1.26 and + 1.45 V, corresponding to Au (110) and Au (111) crystal planes, can be noticed. Moreover, the remarkable increase in the reduction peak at + 0.9 V indicates the enhanced surface area and roughness of the NPAu/GE (black line) compared to that of the bare GE (red line). The electrochemical surface area (ECSA) and the roughness factor (Rf) of both GE and NPAu/GE were calculated [23]. The values were found to be 1.17 cm^2 and 106 for NPAu/GE, and 0.11 cm^2 and 10 for GE, respectively. Hence, these results reveal a 10-fold enhancement in ECSA and Rf for NPAu/GE in comparison to bare GE.

Catechol has a reversible electron-transfer process, so this compound is largely used as a probe to study electrode surface properties during modification steps. Fig. 3 B) shows CVs recorded in 0.1 mol L^{-1} acetic/acetate buffer pH 4.50 with the bare GE (Blank - blue line), and in 1 mmol L^{-1} catechol in 0.1 mol L^{-1} acetic/acetate

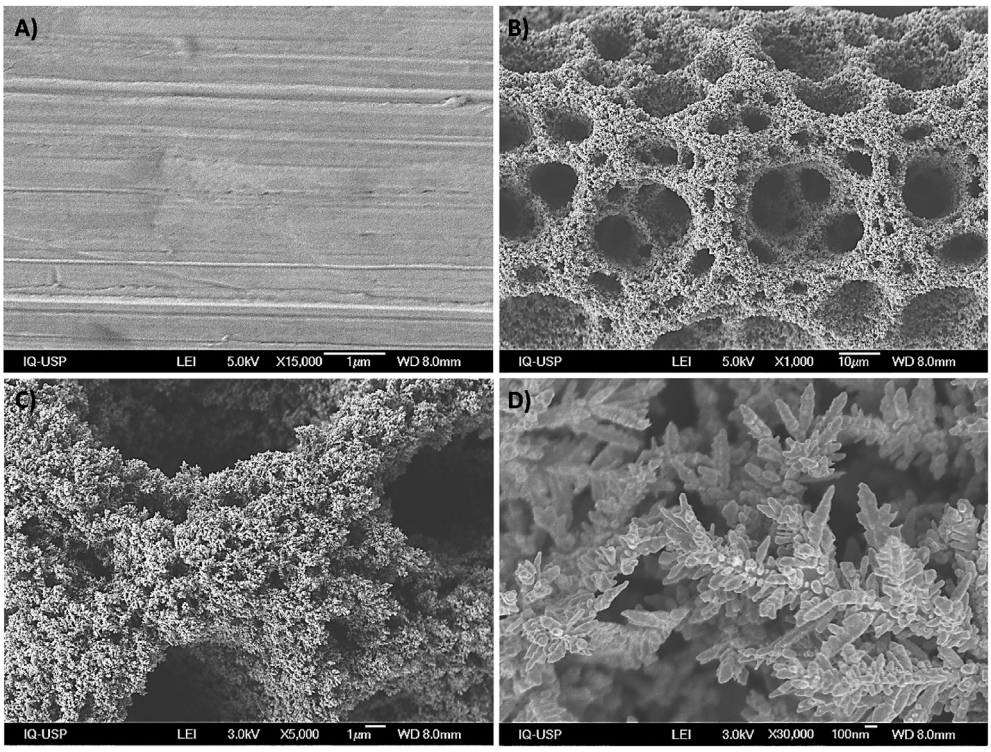

Fig. 2. SEM micrographs of the A) GE, and B), C) and D) NPAu/GE film at different magnifications.

buffer pH 4.50 with a bare GE (red line) and an NPAu/GE (black line), at 75 mV s^{-1} scan rate. As expected, no faradaic process was noticed in the voltammogram recorded in supporting electrolyte (Fig. 3 B), blue line). On the other hand, a well-defined voltammogram characteristics of a diffusion-controlled redox process involving the couple catechol/quinone was observed for the bare GE, whereas enlarged peak currents (oxidation and reduction) with a slight shift to more positive potentials were noticed in the voltammogram recorded with the NPAu/GE. The higher current response for the voltammogram recorded with the NPAu/GE can be attributed to the increased electroactive surface area and the excellent electrical conductivity of the nanoporous structure. Moreover, the enhanced electrocatalytic activity explained by the increasing number of active sites (owing to the presence of dendritic structures and the porous rough surface) also plays a key role in the electron-transfer step. As a result, quinone can be detected according to the reaction shown in Scheme 2 with increased sensitivity, reinforcing the usefulness of the Au nanoporous modification.

The Randles-Sevcik equation describes the effect of scan ate on the peak current in cyclic voltammetry experiments, and Fig. 3C) shows the results obtained with the NPAu/GE in 1 mmol L^{-1} catechol +0.1 mol L^{-1} acetic/acetate buffer pH 4.50. The linear relationship between the redox peak current values and the square root of the scan rate is shown in Fig. 3 D), which indicates that catechol oxidation to quinone at the NPAu/GE is a diffusion-controlled electron-transfer process. This is also confirmed by analyzing the peak-to-peak separation (around 70 mV) and the ratio between anodic and cathodic peak current values (close to 1).

3.3. Optimization of experimental parameters for the fabrication of the NPAu/GE

The experimental parameters for SOX-2 determination were optimized using a 15 ng mL^{-1} SOX-2 standard solution. The electrodeposition of the nanoporous gold layer on the gold electrode surface depends on both deposition time (T_{dep}) and deposition potential (E_{dep}) parameters, which were optimized to obtain the best analytical performance. Experiments regarding the T_{dep} optimization were performed at E_{dep} = − 0.4 V, and T_{dep} was changed from 25 to 200 s. Fig. S3 A) shows that the current increases when the T_{dep} increases until 150 s. Current remained constant for higher T_{dep} values, hence a T_{dep} of 150 s was used as optimum.

E_{dep} was also optimized from − 0.5 to − 5.0 V at a fixed T_{dep} = 150 s. As shown in Fig. S3 B), the current values increased significantly when the applied potential was more negative up to − 4 V, and then remained constant between − 4 and − 5 V. Therefore, T_{dep} = 150 s and E_{dep} = − 4 V were used as optimized parameters in all measurements.

Other important parameters, such as pH buffer, microfluidic flow rate, among others, were optimized according to a previously reported article [30]. Parameters like capture antibody concentration and secondary enzyme marked antibody concentration were used by following the ELISA manufacture parameters.

3.4. Analytical performance of the microfluidic electrochemical immunosensor

The immunosensor analytical performance was analyzed varying the SOX-2 concentration from 0.01 to 50 ng mL^{-1}, in comparison with the commercial ELISA kit test. a linear correlation was observed from 0.11 to 30 ng mL^{-1} and 0.94–15 ng mL^{-1} for the immunosensor (Fig. 4 A) and the ELISA (Fig. 4 B), respectively. The calibration plots followed the equations $\Delta I\ (nA) = 1.17 + 12.1\ C_{SOX\text{-}2}$ with a correlation coefficient of 0.997 for the immunosensor, and $\Delta A\ (O.D.) = -0.046 + 0.042\ C_{SOX\text{-}2}$ with a correlation coefficient of 0.995 for the ELISA, where Δ is the difference between standard and blank solution signals.

The coefficient of variation (CV %) for the determination of

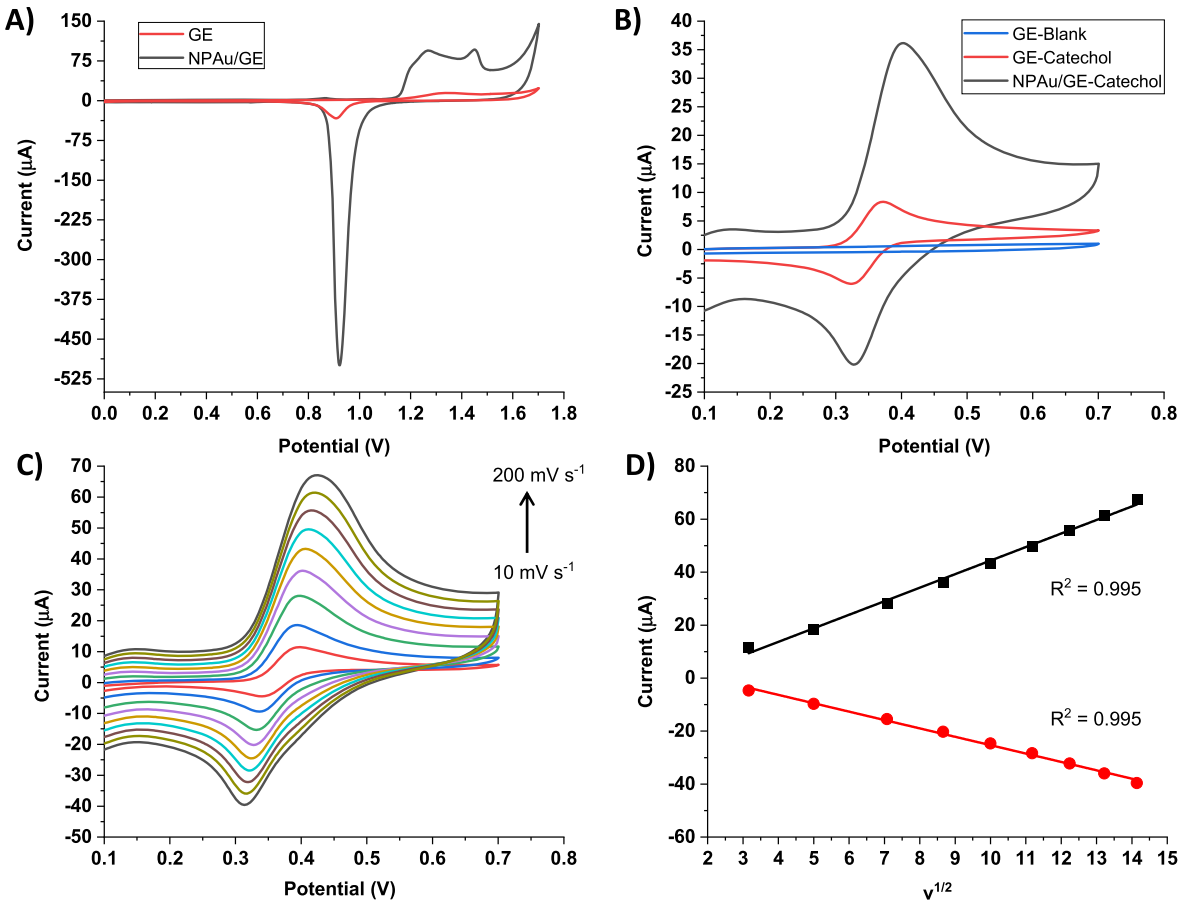

Fig. 3. A) CVs of the bare GE (red line) and NPAu/GE (black line) recorded in 0.5 mol L^{-1} H_2SO_4 from 0 to +1.7 V at 75 mV s^{-1} scan rate, B) CVs recorded in 0.1 mol L^{-1} acetic/acetate buffer pH 4.50 with the bare GE (Blank - blue line), and in 1 mmol L^{-1} catechol in 0.1 mol L^{-1} acetic/acetate buffer pH 4.50, with bare GE (Red line) and NPAu/GE (Black line), at 75 mV s^{-1} scan rate, C) CVs recorded with the NPAu/GE in 1 mmol L^{-1} catechol + 0.1 mol L^{-1} acetic/acetate buffer pH 4.50 at 10, 25, 50, 75, 100, 125, 150, 175, 200 mV s^{-1}, and D) Dependence of the redox peak current values and the square root of the scan rate ($v^{1/2}$). (For interpretation of the references to color in this figure legend, the reader is referred to the Web version of this article.)

10 ng mL^{-1} SOX-2 was below 4.75% for the immunosensor, whereas such value was 4.92% for the ELISA test (n = 5). These values demonstrate that our microfluidic electrochemical immunosensor (MEI) can be used for SOX-2 quantification in human serum samples. The limit of detection (LD) and the limit of quantification (LQ) were calculated according to the IUPAC recommendations [31]. For the immunosensor, the LQ and LD were 0.11 ng mL^{-1} and 30 pg mL^{-1}, while for the ELISA, LQ and LD the values were 0.94 ng mL^{-1} and 200 pg mL^{-1}. These results show that the sensitivity of the electrochemical method is superior in comparison to the spectrophotometric method.

In order to evaluate the correlation between the results obtained by using the immunosensor and the reference method (ELISA), SOX-2 concentrations were compared in a wide dynamic range. (Fig. 4C) shows the straight line with a slope of 0.998, indicating a good correspondence between both methods. Moreover, the total assay time for SOX-2 quantification was 20 min, less than the 90 min required to perform the ELISA test. Also, the immunosensor can be regenerated by injection of a desorption buffer and further washing with 0.1 mol L^{-1} PBS pH 7.00, allowing to use the device for almost 1 month without significant loss of sensitivity.

The selectivity for SOX-2 determination was studied against a 15 ng mL^{-1} SOX-2 standard solution containing some typical cancer biomarkers (EPCAM, EGFR, CEA, CA 15–3, Claudin 7 and CD81) in 10-fold concentration. As shown in Fig. 4 D), the presence of such biomarkers caused less than 3% change in the analytical signal. The results indicated the strong ability of the immunosensor to avoid interferences, which is explained by the use of specific antibodies and the blocking of nonspecific adsorption.

The precision of the microfluidic electrochemical immunosensor (MEI) was studied with five standards solutions (3.76, 10, 15, 20, 25 ng mL^{-1}) (Table 1). The within-assay precision was assessed by measuring the response in the same day for each sample (n = 5). These series of analyses were repeated for 3 consecutive days to estimate the between-assay precision. The SOX-2 measurement showed good precision, as the CV % within-assay values were below 4.5% and the between-assay values were below 4.7%.

The evaluation of the analytical applicability of the microfluidic electrochemical immunosensor (MEI) was conducted by SOX-2 quantification in five spiked samples under the conditions described in section 2.6. Results were compared with those obtained with the commercial ELISA kit test using the paired *t*-test. The results demonstrated that both methods were statistically equal at a confidence level of 95%, as shown in Table 2. A typical protocol for human serum samples preparation is described in the Supplementary material.

4. Conclusions

This is the first microfluidic electrochemical immunosensor (MEI) for SOX-2 determination. Our analytical approach shows outstanding analytical parameters and is based on the microfluidic

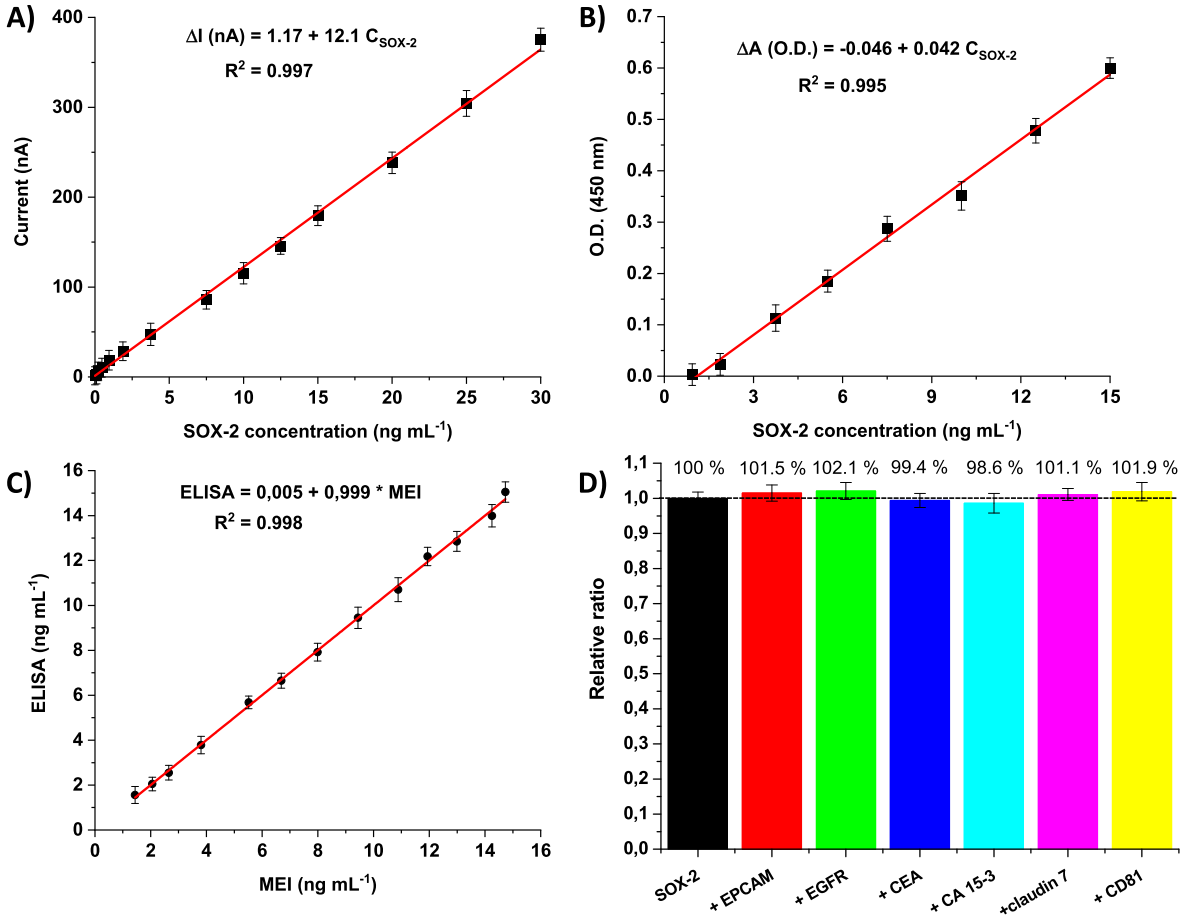

Fig. 4. A) Microfluidic electrochemical immunosensor calibration plot, B) ELISA calibration plot, C) Plot of results obtained with the microfluidic electrochemical immunosensor (MEI) and the ELISA kit for different SOX-2 concentrations, and D) Interference study in the presence of several cancer biomarkers.

Table 1
Within-assay precision and between-assay precision for the SOX-2 microfluidic electrochemical immunosensor.

Samples[a]	Within-assay		Between-assay	
	Mean[b]	CV %	Mean	CV %
3.7	3.6	3.7	3.8	4.2
10	9.9	3.5	10.2	3.1
15	15.2	4.5	14.8	4.7
20	21.2	3.9	19.5	4.2
25	24.7	4.1	25.4	4.5

[a] SOX-2 standard solution (ng mL^{-1}).
[b] Mean of five determinations + S.D.

Table 2
Comparison of SOX-2 concentration values in spiked samples obtained with the developed microfluidic electrochemical immunosensor and the commercial ELISA test.

Samples[a]	MEI[b]	ELISA
0.94	0.95 ± 0.01[c]	0.93 ± 0.02
1.88	1.95 ± 0.05	2.02 ± 0.06
3.76	3.65 ± 0.03	3.89 ± 0.07
7.52	7.39 ± 0.07	7.33 ± 0.08
10	9.9 ± 0.1	10.4 ± 0.2

[a] SOX-2 spiked samples (ng mL^{-1}).
[b] Microfluidic electrochemical immunosensor.
[c] Mean of five determinations + S.D.

channel modification by a physical-chemical treatment in order to obtain an immobilization platform, with high hydrophilicity and increased surface to volume/ratio, which allows the anti-SOX-2 antibody immobilization. In this way, we increased the selectivity and sensitivity of the sandwich immunoassay.

Moreover, the sensitivity of the measurements was enhanced by modifying the gold electrode surface by a dynamic hydrogen bubble template method. The generated gold nanoporous structure (NPAu) platform has outstanding properties, like high specific surface area, large pore volume, uniform nanostructure, good conductivity, and excellent electrochemical activity.

The total assay time employed (20 min) was shorter than the one required for the commercial ELISA (90 min) frequently used. The microfluidic electrochemical immunosensor offered several attractive advantages in comparison with the ELISA, such as high stability, portability, selectivity, reusability, and sensitivity. In conclusion, this device could be used for clinical diagnosis and prognosis of several kinds of carcinomas in human serum samples.

CRediT authorship contribution statement

Matías Regiart: Conceptualization, Methodology, Writing - original draft. **Alba Marina Gimenez:** Validation, Investigation, Visualization. **Alexandre T. Lopes:** Methodology, Investigation. **Marcelo N.P. Carreño:** Visualization, Supervision. **Mauro Bertotti:** Conceptualization, Supervision, Writing - review & editing.

Declaration of competing interest

None.

Acknowledgments

The authors wish to thank the financial support from the Fundação de Amparo à Pesquisa do Estado de São Paulo (FAPESP) (2019/06293–6, 2018/08782–1), and CNPq (306635/2013–5).

Appendix A. Supplementary data

Supplementary data to this article can be found online at https://doi.org/10.1016/j.aca.2020.06.037.

References

[1] D. Novak, L. Hüser, J.J. Elton, V. Umansky, P. Altevogt, J. Utikal, SOX2 in development and cancer biology, Semin. Canc. Biol. (2019), https://doi.org/10.1016/j.semcancer.2019.08.007.
[2] E.P. Metz, A. Rizzino, Sox2 dosage: a critical determinant in the functions of Sox2 in both normal and tumor cells, J. Cell. Physiol. 234 (2019), https://doi.org/10.1002/jcp.28610, 19298–19306.
[3] S. Zhang, Sox2, a key factor in the regulation of pluripotency and neural differentiation, World J. Stem Cell. 6 (2014) 305, https://doi.org/10.4252/wjsc.v6.i3.305.
[4] A. Banerjee, V. Kamath, L. Sundaram, S. Krishnamurthy, OCT4 and SOX2 are reliable markers in detecting stem cells in odontogenic lesions, J. Orofac. Sci. 8 (2016) 16, https://doi.org/10.4103/0975-8844.181920.
[5] K.B. Long, J.L. Hornick, SOX2 is highly expressed in squamous cell carcinomas of the gastrointestinal tract, Hum. Pathol. 40 (2009) 1768–1773, https://doi.org/10.1016/j.humpath.2009.06.006.
[6] Y. Chen, L. Shi, L. Zhang, R. Li, J. Liang, W. Yu, L. Sun, X. Yang, Y. Wang, Y. Zhang, Y. Shang, The molecular mechanism governing the oncogenic potential of SOX2 in breast cancer, J. Biol. Chem. 283 (2008) 17969–17978, https://doi.org/10.1074/jbc.M802917200.
[7] J. Belotte, N.M. Fletcher, M. Alexis, R.T. Morris, A.R. Munkarah, M.P. Diamond, G.M. Saed, Sox2 gene amplification significantly impacts overall survival in serous epithelial ovarian cancer, Reprod. Sci. 22 (2015) 38–46, https://doi.org/10.1177/1933719114542021.
[8] Y. Lu, C. Futtner, J.R. Rock, X. Xu, W. Whitworth, B.L.M. Hogan, M.W. Onaitis, Evidence that SOX2 overexpression is oncogenic in the lung, PloS One 5 (2010), e11022, https://doi.org/10.1371/journal.pone.0011022.
[9] Y. Gen, K. Yasui, Y. Zen, K. Zen, O. Dohi, M. Endo, K. Tsuji, N. Wakabayashi, Y. Itoh, Y. Naito, M. Taniwaki, Y. Nakanuma, T. Okanoue, T. Yoshikawa, SOX2 identified as a target gene for the amplification at 3q26 that is frequently detected in esophageal squamous cell carcinoma, Canc. Genet. Cytogenet. 202 (2010) 82–93, https://doi.org/10.1016/j.cancergencyto.2010.01.023.
[10] X. Jia, X. Li, Y. Xu, S. Zhang, W. Mou, Y. Liu, Y. Liu, D. Lv, C.-H. Liu, X. Tan, R. Xiang, N. Li, SOX2 promotes tumorigenesis and increases the anti-apoptotic property of human prostate cancer cell, J. Mol. Cell Biol. 3 (2011) 230–238, https://doi.org/10.1093/jmcb/mjr002.
[11] Z. Yang, X. Pan, A. Gao, W. Zhu, Expression of Sox2 in cervical squamous cell carcinoma, J. BUON. 19 (2014) 203–206.
[12] M. Stevanovic, D. Drakulic, J. Marjanovic Vicentic, M. Schwirtlich, J. Tosic, A. Krstic, A. Klajn, The overexpression of SOX2 affects the migration of human teratocarcinoma cell line NT2/D1, An. Acad. Bras. Cienc. 87 (2015) 389–405, https://doi.org/10.1590/0001-3765201520140352.
[13] S.S. Yu, N. Cirillo, The molecular markers of cancer stem cells in head and neck tumors, J. Cell. Physiol. 235 (2020) 65–73, https://doi.org/10.1002/jcp.28963.
[14] Z.H. Ren, C.P. Zhang, T. Ji, Expression of SOX2 in oral squamous cell carcinoma and the association with lymph node metastasis (Review), Oncol. Lett. 11 (2016) 1973–1979, https://doi.org/10.3892/ol.2016.4207.
[15] D. Zhang, W. Li, Z. Ma, H. Han, Improved ELISA for tumor marker detection using electro-readout-mode based on label triggered degradation of methylene blue, Biosens. Bioelectron. 126 (2019) 800–805, https://doi.org/10.1016/j.bios.2018.11.038.
[16] H. Filik, A.A. Avan, Nanostructures for nonlabeled and labeled electrochemical immunosensors: simultaneous electrochemical detection of cancer markers: a review, Talanta 205 (2019), 120153, https://doi.org/10.1016/j.talanta.2019.120153.
[17] E.B. Aydın, M.K. Sezgintürk, A sensitive and disposable electrochemical immunosensor for detection of SOX2, a biomarker of cancer, Talanta 172 (2017) 162–170, https://doi.org/10.1016/j.talanta.2017.05.048.
[18] B. Özcan, M.K. Sezgintürk, Highly sensitive and cost-effective ITO-based immunosensor system modified by 11-CUTMS: analysis of SOX2 protein in real human serum, Int. J. Biol. Macromol. 130 (2019) 245–252, https://doi.org/10.1016/j.ijbiomac.2019.02.112.
[19] M. Regiart, M.A. Fernández-Baldo, V.G. Spotorno, F.A. Bertolino, J. Raba, Ultra sensitive microfluidic immunosensor for determination of clenbuterol in bovine hair samples using electrodeposited gold nanoparticles and magnetic micro particles as bio-affinity platform, Biosens. Bioelectron. 41 (2013) 211–217, https://doi.org/10.1016/j.bios.2012.08.020.
[20] Q. Tu, J.C. Wang, Y. Zhang, R. Liu, W. Liu, L. Ren, S. Shen, J. Xu, L. Zhao, J. Wang, Surface modification of poly(dimethylsiloxane) and its applications in microfluidics-based biological analysis, Rev. Anal. Chem. 31 (2012) 177–192, https://doi.org/10.1515/revac-2012-0016.
[21] J. Zhou, D.A. Khodakov, A.V. Ellis, N.H. Voelcker, Surface modification for PDMS-based microfluidic devices, Electrophoresis 33 (2012) 89–104, https://doi.org/10.1002/elps.201100482.
[22] B.J. Plowman, L.A. Jones, S.K. Bhargava, Building with bubbles: the formation of high surface area honeycomb-like films via hydrogen bubble templated electrodeposition, Chem. Commun. 51 (2015) 4331–4346, https://doi.org/10.1039/c4cc06638c.
[23] A. Sukeri, M. Bertotti, Electrodeposited honeycomb-like dendritic porous gold surface: an efficient platform for enzyme-free hydrogen peroxide sensor at low overpotential, J. Electroanal. Chem. 805 (2017) 18–23, https://doi.org/10.1016/j.jelechem.2017.10.004.
[24] A. Kumar, J.M. Gonçalves, A. Sukeri, K. Araki, M. Bertotti, Correlating surface growth of nanoporous gold with electrodeposition parameters to optimize amperometric sensing of nitrite, Sensor. Actuator. B Chem. 263 (2018) 237–247, https://doi.org/10.1016/j.snb.2018.02.125.
[25] M. Regiart, M.A. Fernández-Baldo, J. Villarroel-Rocha, G.A. Messina, F.A. Bertolino, K. Sapag, A.T. Timperman, J. Raba, Microfluidic immunosensor based on mesoporous silica platform and CMK-3/poly-acrylamide-co-methacrylate of dihydrolipoic acid modified gold electrode for cancer biomarker detection, Anal. Chim. Acta 963 (2017) 83–92, https://doi.org/10.1016/j.aca.2017.01.029.
[26] A. Kumar, V.L. Furtado, J.M. Gonçalves, R. Bannitz-Fernandes, L.E.S. Netto, K. Araki, M. Bertotti, Amperometric microsensor based on nanoporous gold for ascorbic acid detection in highly acidic biological extracts, Anal. Chim. Acta 1095 (2020) 61–70, https://doi.org/10.1016/j.aca.2019.10.022.
[27] S. Kuddannaya, Y.J. Chuah, M.H.A. Lee, N.V. Menon, Y. Kang, Y. Zhang, Surface chemical modification of poly(dimethylsiloxane) for the enhanced adhesion and proliferation of mesenchymal stem cells, ACS Appl. Mater. Interfaces 5 (2013) 9777–9784, https://doi.org/10.1021/am402903e.
[28] L.M. Johnson, L. Gao, C. Shields IV, M. Smith, K. Efimenko, K. Cushing, J. Genzer, G.P. López, Elastomeric microparticles for acoustic mediated bioseparations, J. Nanobiotechnol. 11 (2013) 22, https://doi.org/10.1186/1477-3155-11-22.
[29] J. Lee, J. Kim, H. Kim, Y.M. Bae, K.H. Lee, H.J. Cho, Effect of thermal treatment on the chemical resistance of polydimethylsiloxane for microfluidic devices, J. Micromech. Microeng. 23 (2013), 0350007, https://doi.org/10.1088/0960-1317/23/3/035007.
[30] C.F. Jofre, M. Regiart, M.A. Fernández-Baldo, M. Bertotti, J. Raba, G.A. Messina, Electrochemical microfluidic immunosensor based on TES-AuNPs@Fe3O4 and CMK-8 for IgG anti-Toxocara canis determination, Anal. Chim. Acta 1096 (2020) 120–129, https://doi.org/10.1016/j.aca.2019.10.040.
[31] L.A. Currie, Nomenclature in evaluation of analytical methods including detection and quantification capabilities (IUPAC Recommendations 1995), Anal. Chim. Acta 391 (1999) 105–126, https://doi.org/10.1016/S0003-2670(99)00104-X.